Convergence and superconvergence of staggered discontinuous Galerkin methods for the three-dimensional Maxwell's equations on Cartesian grids

Eric T. Chung, Patrick Ciarlet and Tang Fei Yu

Department of Mathematics, The Chinese University of Hong Kong, Hong Kong SAR
Laboratoire POEMS, UMR 7231 CNRS/ENSTA/INRIA, ENSTA ParisTech, Paris, France

Abstract

In this paper, a new type of staggered discontinuous Galerkin methods for the three dimensional Maxwell's equations is developed and analyzed. The spatial discretization is based on staggered Cartesian grids so that many good properties are obtained. First of all, our method has the advantages that the numerical solution preserves the electromagnetic energy and automatically fulfills a discrete version of the Gauss law. Moreover, the mass matrices are diagonal, thus time marching is explicit and is very efficient. Our method is high order accurate and the optimal order of convergence is rigorously proved. It is also very easy to implement due to its Cartesian structure and can be regarded as a generalization of the classical Yee's scheme as well as the quadrilateral edge finite elements. Furthermore, a superconvergence result, that is the convergence rate is one order higher at interpolation nodes, is proved. Numerical results are shown to confirm our theoretical statements, and applications to problems in unbounded domains with the use of PML are presented.

Key words: Staggered discontinuous Galerkin method, Maxwell's equations, energy conservation, Gauss law, optimal convergence, superconvergence, Yee's scheme, edge element method

1. Introduction

In this paper, we will develop and mathematically analyze a new class of staggered discontinuous Galerkin (DG) methods for the time-dependent Maxwell's equations in three space dimensions. We will construct a class of methods that will provide the following advantages:

(1) high order accurate,
(2) optimal rate of convergence,
(3) conservation of the electromagnetic energy,
(4) diagonal mass matrix, and
(5) automatic fulfillment of a discrete Gauss law.

We start with a description of the problem setting. Let Ω be a bounded domain in $\mathbb{R}^3$ and $T > 0$ be a fixed time. We consider the following Maxwell's equations

$$\varepsilon \frac{\partial \boldsymbol{E}}{\partial t} - \nabla \times \boldsymbol{H} = -\boldsymbol{J}, \qquad \boldsymbol{x} \in \Omega, \quad t \in (0, T), \tag{1}$$

$$\mu \frac{\partial \boldsymbol{H}}{\partial t} + \nabla \times \boldsymbol{E} = \boldsymbol{0}, \qquad \boldsymbol{x} \in \Omega, \quad t \in (0, T), \tag{2}$$

where $\boldsymbol{E}$ and $\boldsymbol{H}$ are the electric and magnetic fields to be approximated, $\boldsymbol{J}$ is the given current density, ε and μ are the electric permittivity and the magnetic permeability respectively. Throughout the paper, vectors are denoted by bold face. The above problem is equipped with the perfect conductor boundary condition $\boldsymbol{E} \times \boldsymbol{n} = \boldsymbol{0}$ on $\partial\Omega$ as well as initial conditions. Furthermore, the exterior problem for the above Maxwell's equations will be considered, for which our method coupled with the perfectly matched layer (PML) will be used. In this case, Ω represents the computational domain which contains the absorbing layers, see Berenger [1]. The main significance of this paper is the spatial discretization of (1)-(2) on staggered Cartesian grids, which will give the above desirable properties.

The study of numerical solutions of partial differential equations by the DG methods is a very active research topic, see for example Brezzi, Marini & Süli [3] for the application of DG method to the first order hyperbolic system, Gittelson, Hiptmair & Perugia [19] for the helmholtz equation and Cockburn & Shu [14] for the convection-diffusion equation. DG methods for the time dependent Maxwell's equations are widely studied in literature. For instance, upwind type DG and central type DG are proposed and analyzed in Hesthaven & Warburton [21] and Fezoui, Lanteri, Lohrengel & Piperno [18] respectively. In Grote, Schneebeli & Schötzau [20], the optimal convergence and energy conservation for the interior penalty DG are proved. Besides, many DG methods are developed and analyzed for the time harmonic Maxwell's equations and the Maxwell eigenvalue problem, see for example Brenner, Li & Sung [2], Buffa, Houston & Perugia [4], Buffa & Perugia [5], Costabel & Dauge [16], Dauge [17], Houston, Perugia, Schneebeli & Schötzau [23, 24], Houston, Perugia & Schötzau [25], Perugia, Schötzau & Monk [30] and Chung & Lee [11].

Recently, a new class of DG methods based on a non-standard type of staggered grid is introduced in Chung & Engquist [9, 10] for the wave equations, in Chung & Lee [11] for the curl-curl operator and in Chung & Lee [12] for the convection-diffusion equation. Moreover, wave transmission problems in the interface between classical material and meta-material using this kind of method is proposed and analyzed in Chung & Ciarlet [6]. These methods have the advantages that the structures, such as energy and density, arising from the partial differential equations are preserved. Moreover, for time-dependent problems, the resulting mass matrices are block diagonal. The lowest order version of these methods is also related to the co-volume method, see Chung, Du & Zou [7], Chung & Engquist [8], and the classical Yee's scheme, see Yee [31]. In this paper, we will develop a new numerical method for the time-dependent Maxwell's equations based on this new staggered grid idea. We emphasize that, there are many methods in literature, but as far as we know, the method proposed in this paper is the first one that all the above desirable properties are proved. We will develop two types of staggered DG elements. For the first type, different components of the electric and magnetic fields will be approximated by different orders of polynomials, similar to the Nedelec's first family, see Nedelec [28], Hiptmair [22] and Monk [27]. The second type uses the same polynomial order for all components of electric and magnetic fields, similar to the Nedelec's second family, see Nedelec [29]. One of the key differences is that our element is globally discontinuous with local tangential continuity, contrary to the global tangential continuity of Nedelec's elements. Another difference is that our element is defined on staggered grids. All these differences result in the above advantages. Furthermore, a distinctive feature of our method is that we use a combination of Gaussian points and Radau points as interpolation points which gives diagonal mass matrix as well as energy conservation. Related work using Gauss point mass-lumping can be found in Cohen & Monk [15].

In addition, we will prove a superconvergence result, which states that the convergence rate is one order higher at the interpolation points. For elliptic problem, a related result is proved in Cockburn, Kanschat, Perugia & Schötzau [13]. For Maxwell's equations with Nedelec first type elements, superconvergence is shown for the lowest order case in Huang, Li, Yang & Sun [26]. In

this paper, we will prove a superconvergence result for arbitrary order of approximation polynomial.

The paper is organized as follows. In Section 2, we will introduce the new staggered DG space, and in Section 3, we will give the method derivation. The conservation of electromagnetic energy and discrete Gauss law will be proved in Section 4. The convergence and superconvergence of our method are proved in Section 5. In Section 6, numerical results are presented to validate our theoretical estimates and the use of PML for unbounded domain problem is shown.

2. Staggered DG Spaces

In this section, we will give the definitions of our staggered Cartesian grids as well as the staggered DG finite element spaces. These spaces retain some good properties of the classical Nedelec edge finite element spaces of the first and second types introduced in Nedelec [28, 29] and at the same time give more advantages. Furthermore, we will give a brief review of Gaussian and Radau points which are used as interpolation points. These are the key ingredients that give diagonal mass matrices and energy conservation.

We consider a rectangular domain $\Omega = [0, L]^3$ on which a rectangular grid is defined with mesh sizes h_1, h_2 and h_3 respectively in x, y and z directions. The nodal points x_i, y_j, z_k are defined by $x_i = ih_1, y_j = jh_2$ and $z_k = kh_3$, $i, j, k = 0, 1, 2, \cdots$. We call this rectangular grid the *initial grid*. The finite element basis functions of $\boldsymbol{H}$ and $\boldsymbol{E}$ are defined on *staggered grids* derived from the initial grid. For that, we need mid-points, with coordinates defined by $x_{i\pm\frac{1}{2}} = (i \pm \frac{1}{2})h_1$, $y_{j\pm\frac{1}{2}} = (j \pm \frac{1}{2})h_2$, $z_{k\pm\frac{1}{2}} = (k \pm \frac{1}{2})h_3$. We emphasize that different components of $\boldsymbol{H}$ and $\boldsymbol{E}$ are defined on different staggered grids.

Let $p, p_1, p_2, p_3 \geq 0$ be non-negative integers. We use the notation Q_{p_1,p_2,p_3} to represent the space of polynomials of degree p_1 for x-variable, degree p_2 for the y-variable and degree p_3 for the z-variable. If $p = p_1 = p_2 = p_3$, we write $Q_{p,p,p} = Q_p$. Moreover, we let $h = \max(h_1, h_2, h_3)$.

To begin the description of our new DG method, we will first review the definitions of Gauss-Radau points and Gauss-Radau quadrature. Let $p \geq 0$. Consider the interval $[0, h]$. The Gauss-Radau quadrature points $0 = \xi_0 < \xi_1 < \xi_2 < \cdots < \xi_p < h$ and the positive weights $w_0, w_1, w_2, \cdots, w_p$ are defined so that the following integration rule

$$\int_0^h f(\xi)\, d\xi = h \sum_{i=0}^{p} w_i f(\xi_i)$$

is exact for all polynomials of degree less than or equal to $2p$. The above formula is called the Gauss-Radau quadrature. Furthermore, we will use these points as interpolation points to define our basis functions. In particular, for a given i, $i = 0, 1, \cdots, p$, we define by $\eta_{p,i}(\xi)$ the unique polynomial of degree p such that $\eta_{p,i}(\xi_i) = 1$ and $\eta_{p,i}(\xi_{i'}) = 0$ for $i' \neq i$. One distinctive advantage is that these basis functions are orthogonal since by the Gauss-Radau quadrature we have

$$\int_0^h \eta_{p,i}(\xi)\, \eta_{p,i'}(\xi)\, d\xi = h \sum_{i''=0}^{p} w_i \eta_{p,i}(\xi_{i''})\, \eta_{p,i'}(\xi_{i''}) = h w_i \delta_{ii'}$$

where $\delta_{ii'} = 1$ if $i' = i$ and $\delta_{ii'} = 0$ if $i' \neq i$.

Let $p \geq 1$. The Gaussian quadrature points $0 < \gamma_1 < \gamma_2 < \cdots < \gamma_p < h$ and the positive weights $c_1, c_2, \cdots, c_p$ are defined so that the following integration rule

$$\int_0^h f(\gamma)\, d\gamma = h \sum_{i=1}^{p} c_i f(\gamma_i)$$

is exact for all polynomials of degree less than or equal to $2p-1$. The above formula is called the Gaussian quadrature. Furthermore, we will use these points as interpolation points to define our basis functions. In particular, for a given i, $i = 1, \cdots, p$, we define by $\lambda_{p,i}(\gamma)$ the unique polynomial of degree $p-1$ such that $\lambda_{p,i}(\gamma_i) = 1$ and $\lambda_{p,i}(\gamma_{i'}) = 0$ for $i' \neq i$. One distinctive advantage is that these basis functions are orthogonal since by the Gaussian quadrature we have

$$\int_0^h \lambda_{p,i}(\gamma)\, \lambda_{p,i'}(\gamma)\, d\gamma = h \sum_{i''=1}^{p} c_i \lambda_{p,i}(\gamma_{i''})\, \lambda_{p,i'}(\gamma_{i''}) = h c_i \delta_{ii'}.$$

Our basis functions are defined by using interpolation points obtained from some tensor products of the above points. Consider a reference element $\hat{\tau} = [-h, h]^3$. In $\hat{\tau}$, we define two types of interpolation points, which are symmetric about the origin $(0, 0, 0)$.

First type interpolation points:

We take $p \geq 1$. We will define three sets of interpolation points $S_1^{(1)}, S_2^{(1)}$ and $S_3^{(1)}$. $S_1^{(1)}$ is defined by the tensor product of

$$\{-\gamma_p, \cdots - \gamma_1, \gamma_1, \cdots, \gamma_p\} \times \{-\xi_p, \cdots, -\xi_1, 0, \xi_1, \cdots, \xi_p\} \times \{-\xi_p, \cdots, -\xi_1, 0, \xi_1, \cdots, \xi_p\}.$$

Similarly $S_2^{(1)}$ and $S_3^{(1)}$ are defined by the tensor products of

$$\{-\xi_p, \cdots, -\xi_1, 0, \xi_1, \cdots, \xi_p\} \times \{-\gamma_p, \cdots - \gamma_1, \gamma_1, \cdots, \gamma_p\} \times \{-\xi_p, \cdots, -\xi_1, 0, \xi_1, \cdots, \xi_p\}.$$

and

$$\{-\xi_p, \cdots, -\xi_1, 0, \xi_1, \cdots, \xi_p\} \times \{-\xi_p, \cdots, -\xi_1, 0, \xi_1, \cdots, \xi_p\} \times \{-\gamma_p, \cdots - \gamma_1, \gamma_1, \cdots, \gamma_p\}.$$

respectively.

Second type interpolation points:

We take $p \geq 0$. We will define three sets of interpolation points $S_1^{(2)}, S_2^{(2)}$ and $S_3^{(2)}$. $S_1^{(2)}$ is defined by the tensor product of

$$\{-\gamma_{p+1}, \cdots - \gamma_1, \gamma_1, \cdots, \gamma_{p+1}\} \times \{-\xi_p, \cdots, -\xi_1, 0, \xi_1, \cdots, \xi_p\} \times \{-\xi_p, \cdots, -\xi_1, 0, \xi_1, \cdots, \xi_p\}.$$

Similarly $S_2^{(2)}$ and $S_3^{(2)}$ are defined by the tensor products of

$$\{-\xi_p, \cdots, -\xi_1, 0, \xi_1, \cdots, \xi_p\} \times \{-\gamma_{p+1}, \cdots - \gamma_1, \gamma_1, \cdots, \gamma_{p+1}\} \times \{-\xi_p, \cdots, -\xi_1, 0, \xi_1, \cdots, \xi_p\}.$$

and

$$\{-\xi_p, \cdots, -\xi_1, 0, \xi_1, \cdots, \xi_p\} \times \{-\xi_p, \cdots, -\xi_1, 0, \xi_1, \cdots, \xi_p\} \times \{-\gamma_{p+1}, \cdots - \gamma_1, \gamma_1, \cdots, \gamma_{p+1}\}.$$

respectively. We remark that the superscripts in the above definitions denote the type of interpolation points. The main difference between the above two types of interpolation points is that we use one more Gaussian point in the second type for the same value of p.

With the above two types of interpolation points, we will define the finite element spaces for $\boldsymbol{H} = (H_1, H_2, H_3)^t$. As they will be illustrated below, the finite element functions for $\boldsymbol{H}$ are defined with respect to faces. Thus, we will call these high order *face* basis functions. These are also related to the $H(\mathrm{div})$-conforming finite elements, see Nedelec [28, 29].

We begin by the definition of the finite element space U_1 for the component H_1. Consider a face κ of the initial grid that has normal direction parallel to the x-axis. We write

$$\kappa = \{\, x = x_i,\ y_j \leq y \leq y_{j+1},\ z_k \leq z \leq z_{k+1}\}.$$

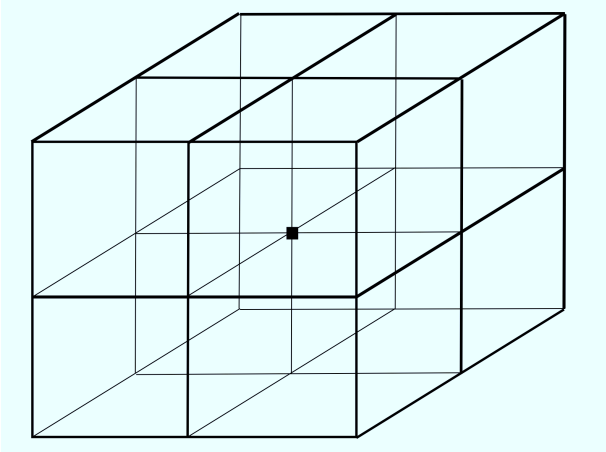

Figure 1: A macro cell $\tau_1(\kappa)$ with center point denoted by black square. This macro cell is sub-divided into 8 sub-cells.

Then, associated to the face κ, we define a cell $\tau_1(\kappa)$ as follows:

$$\tau_1(\kappa) = [x_{i-\frac{1}{2}}, x_{i+\frac{1}{2}}] \times [y_j, y_{j+1}] \times [z_k, z_{k+1}].$$

Correspondingly, our basis functions for H_1 will have support on $\tau_1(\kappa)$, for each face κ that has normal direction parallel to the x-axis. Each $\tau_1(\kappa)$ is called a *macro cell* and is divided into 8 rectangular subregions, called *sub-cells*, by using the center point $(x_i, y_{j+\frac{1}{2}}, z_{k+\frac{1}{2}})$, and 12 internal faces parallel to the faces of $\tau_1(\kappa)$, see Fig 1. The space U_1 is then defined as the space of functions whose restriction to each macro cell $\tau_1(\kappa)$ are piecewise polynomials with additional continuity requirement on the internal faces. Note that there is no continuity requirement on the faces between two macro cells. We will define two types of staggered DG spaces based on the two types of interpolation points defined above.

- **First type basis functions for first component**

  For $p \geq 1$, these functions are piecewise polynomial on each macro cell $\tau_1(\kappa)$ that belong to $Q_{p-1,p,p}$ in each of the 8 sub-cells with the additional requirement that they are continuous on the 8 (out of 12) internal faces of $\tau_1(\kappa)$ that are parallel to the x-axis. If the macro cell $\tau_1(\kappa)$ is mapped to the reference element $\hat{\tau}$ with the center of $\tau_1(\kappa)$ mapped to the origin of $\hat{\tau}$, then these functions can be defined via the interpolation points $S_1^{(1)}$. Thus, inside each macro cell, the functions are continuous with respect to the y and z variables while discontinuous with respect to the x variable.

- **Second type basis functions for first component**

  For $p \geq 0$, these functions are piecewise polynomial on each macro cell $\tau_1(\kappa)$ that belong to Q_p in each of the 8 sub-cells with the additional requirement that they are continuous on the 8 (out of 12) internal faces of $\tau_1(\kappa)$ that are parallel to the x-axis. If the macro cell $\tau_1(\kappa)$ is mapped to the reference element $\hat{\tau}$ with the center of $\tau_1(\kappa)$ mapped to the origin of $\hat{\tau}$, then these functions can be defined via the interpolation points $S_1^{(2)}$. Thus, inside each macro cell, the functions are continuous with respect to the y and z variables while discontinuous with respect to the x variable.

Next, we define the finite element space U_2 for the component H_2. To do so, we consider a face κ that has normal direction parallel to the y-axis:

$$\kappa = \{x_i \le x \le x_{i+1},\ y = y_j,\ z_k \le z \le z_{k+1}\ \},$$

and introduce the corresponding macro cell $\tau_2(\kappa)$ by

$$\tau_2(\kappa) = [x_i, x_{i+1}] \times [y_{j-\frac{1}{2}}, y_{j+\frac{1}{2}}] \times [z_k, z_{k+1}].$$

This macro cell is then divided into 8 rectangular sub-cells by using the center point $(x_{i+\frac{1}{2}}, y_j, z_{k+\frac{1}{2}})$. The space U_2 is then defined as the space of functions whose restriction to each macro cell $\tau_2(\kappa)$ are piecewise polynomials with additional requirement on continuity on internal faces. Note that there is no continuity requirement on the faces between two macro cells. We will define two types of staggered DG spaces based on the two types of interpolation points defined above.

- **First type basis functions for second component**

  For $p \ge 1$, these functions are piecewise polynomial on each macro cell $\tau_2(\kappa)$ that belong to $Q_{p,p-1,p}$ in each of the 8 sub-cells with the additional requirement that they are continuous on the 8 (out of 12) internal faces of $\tau_2(\kappa)$ that are parallel to the y-axis. If the macro cell $\tau_2(\kappa)$ is mapped to the reference element $\hat{\tau}$ with the center of $\tau_2(\kappa)$ mapped to the origin of $\hat{\tau}$, then these functions can be defined via the interpolation points $S_2^{(1)}$. Thus, inside each macro cell, the functions are continuous with respect to the x and z variables while discontinuous with respect to the y variable.

- **Second type basis functions for second component**

  For $p \ge 0$, these functions are piecewise polynomial on each macro cell $\tau_2(\kappa)$ that belong to Q_p in each of the 8 sub-cells with the additional requirement that they are continuous on the 8 (out of 12) internal faces of $\tau_2(\kappa)$ that are parallel to the y-axis. If the macro cell $\tau_2(\kappa)$ is mapped to the reference element $\hat{\tau}$ with the center of $\tau_2(\kappa)$ mapped to the origin of $\hat{\tau}$, then these functions can be defined via the interpolation points $S_2^{(2)}$. Thus, inside each macro cell, the functions are continuous with respect to the x and z variables while discontinuous with respect to the y variable.

Finally, we define the finite element space U_3 for the component H_3. We consider a face κ that has normal direction parallel to the z-axis:

$$\kappa = \{\ x_i \le x \le x_{i+1},\ y_j \le y \le y_{j+1},\ z = z_k\ \},$$

and introduce the corresponding macro cell $\tau_3(\kappa)$ by

$$\tau_3(\kappa) = [x_i, x_{i+1}] \times [y_j, y_{j+1}] \times [z_{k-\frac{1}{2}}, z_{k+\frac{1}{2}}].$$

This macro cell is then divided into 8 rectangular sub-cells by using the center point $(x_{i+\frac{1}{2}}, y_{j+\frac{1}{2}}, z_k)$. The space U_3 is then defined as the space of functions whose restriction to each macro cell $\tau_3(\kappa)$ are piecewise polynomials with additional requirement on internal faces. Note that there is no continuity requirement on the faces between two macro cells. We will define two types of staggered DG spaces based on the two types of interpolation points defined above.

- **First type basis functions for third component**

  For $p \geq 1$, these functions are piecewise polynomial on each macro cell $\tau_3(\kappa)$ that belong to $Q_{p,p,p-1}$ in each of the 8 sub-cells with the additional requirement that they are continuous on the 8 (out of 12) internal faces of $\tau_3(\kappa)$ that are parallel to the z-axis. If the macro cell $\tau_3(\kappa)$ is mapped to the reference element $\hat{\tau}$ with the center of $\tau_3(\kappa)$ mapped to the origin of $\hat{\tau}$, then these functions can be defined via the interpolation points $S_3^{(1)}$. Thus, inside each macro cell, the functions are continuous with respect to the x and y variables while discontinuous with respect to the z variable.

- **Second type basis functions for third component**

  For $p \geq 0$, these functions are piecewise polynomial on each macro cell $\tau_3(\kappa)$ that belong to Q_p in each of the 8 sub-cells with the additional requirement that they are continuous on the 8 (out of 12) internal faces of $\tau_3(\kappa)$ that are parallel to the z-axis. If the macro cell $\tau_3(\kappa)$ is mapped to the reference element $\hat{\tau}$ with the center of $\tau_3(\kappa)$ mapped to the origin of $\hat{\tau}$, then these functions can be defined via the interpolation points $S_3^{(2)}$. Thus, inside each macro cell, the functions are continuous with respect to the x and y variables while discontinuous with respect to the z variable.

Next, we will give the definitions of the finite element spaces for $\boldsymbol{E} = (E_1, E_2, E_3)^t$. These spaces are defined with respect to edges. Thus, they are called high order *edge* basis functions. These are also related to the $H(\mathrm{curl})$-conforming finite elements, see Nedelec [28, 29].

We first give the definition of the finite element space W_1 for the component E_1. Consider an edge σ that is parallel to the x-axis. We write

$$\sigma = \{\, x_i \leq x \leq x_{i+1},\ y = y_j,\ z = z_k \,\}.$$

Then we define the corresponding macro cell $\tau_1(\sigma)$:

$$\tau_1(\sigma) = [x_i, x_{i+1}] \times [y_{j-\frac{1}{2}}, y_{j+\frac{1}{2}}] \times [z_{k-\frac{1}{2}}, z_{k+\frac{1}{2}}].$$

This macro cell is then divided into 8 rectangular sub-cells by using the center point $(x_{i+\frac{1}{2}}, y_j, z_k)$. We also consider two types of staggered DG spaces. The space W_1 is defined in the same way as U_1.

To define the finite element space W_2 for E_2, we consider an edge σ that is parallel to the y-axis, and write

$$\sigma = \{\, x = x_i,\ y_j \leq y \leq y_{j+1},\ z = z_k \,\},$$

and define the corresponding macro cell $\tau_2(\sigma)$:

$$\tau_2(\sigma) = [x_{i-\frac{1}{2}}, x_{i+\frac{1}{2}}] \times [y_j, y_{j+1}] \times [z_{k-\frac{1}{2}}, z_{k+\frac{1}{2}}].$$

The space W_2 is defined in the same way as U_2.

Likewise, for the finite element space W_3 for E_3, we take an edge σ that is parallel to the z-axis, and write

$$\sigma = \{\, x = x_i,\ y = y_j,\ z_k \leq z \leq z_{k+1} \,\},$$

we define the corresponding macro cell $\tau_3(\sigma)$:

$$\tau_3(\sigma) = [x_{i-\frac{1}{2}}, x_{i+\frac{1}{2}}] \times [y_{j-\frac{1}{2}}, y_{j+\frac{1}{2}}] \times [z_k, z_{k+1}].$$

The space W_3 is defined in the same way as U_3.

3. Method derivation

In this section, we will give a detail derivation of our new staggered DG method for the Maxwell's equations (1)-(2).

First, we recall that $\tau_1(\kappa), \tau_2(\kappa)$ and $\tau_3(\kappa)$ are defined as the macro cells with respect to the faces of the initial grid that have normal direction parallel to the x-, y- and z-axis respectively. To derive our new staggered DG method, the key idea is to obtain an integral form of the Maxwell's equations on these staggered macro cells. We take a test function $\boldsymbol{\phi} = (\phi_1, 0, 0)^t$ with $\phi_1 \in U_1$, multiply (2) by it and integrate the resulting equation over a macro cell $\tau_1(\kappa)$ to obtain

$$\int_{\tau_1(\kappa)} \mu \frac{\partial H_1}{\partial t}\, \phi_1 \, d\boldsymbol{x} + \Big\{ \int_{\tau_1(\kappa)} (E_2 \frac{\partial \phi_1}{\partial z} - E_3 \frac{\partial \phi_1}{\partial y})\, d\boldsymbol{x} - \int_{\partial\tau_1(\kappa)} (E_2 n_3 - E_3 n_2)\phi_1 \, ds \Big\} = 0\,. \tag{3}$$

Replacing the exact solution H_1 by the numerical approximation H_1^h, we get

$$\int_{\tau_1(\kappa)} \mu \frac{\partial H_1^h}{\partial t}\, \phi_1 \, d\boldsymbol{x} + \Big\{ \int_{\tau_1(\kappa)} (E_2^h \frac{\partial \phi_1}{\partial z} - E_3^h \frac{\partial \phi_1}{\partial y})\, d\boldsymbol{x} - \int_{\partial\tau_1(\kappa)} (E_2^h n_3 - E_3^h n_2)\phi_1 \, ds \Big\} = 0\,. \tag{4}$$

To simplify notations, we define

$$B_{\tau_1(\kappa)}(\boldsymbol{E}^h, \boldsymbol{\phi}) = \int_{\tau_1(\kappa)} (E_2^h \frac{\partial \phi_1}{\partial z} - E_3^h \frac{\partial \phi_1}{\partial y})\, d\boldsymbol{x} - \int_{\partial\tau_1(\kappa)} (E_2^h n_3 - E_3^h n_2)\phi_1 \, ds.$$

In the same way, we multiply (2) by a test function $\boldsymbol{\phi} = (0, \phi_2, 0)^t$ with $\phi_2 \in U_2$, integrate the resulting equation on a macro cell $\tau_2(\kappa)$ and finally replace exact solutions by DG solutions to obtain

$$\int_{\tau_2(\kappa)} \mu \frac{\partial H_2^h}{\partial t}\, \phi_2 \, d\boldsymbol{x} + \Big\{ \int_{\tau_2(\kappa)} (E_3^h \frac{\partial \phi_2}{\partial x} - E_1^h \frac{\partial \phi_2}{\partial z})\, d\boldsymbol{x} - \int_{\partial\tau_2(\kappa)} (E_3^h n_1 - E_1^h n_3)\phi_2 \, ds \Big\} = 0. \tag{5}$$

We define

$$B_{\tau_2(\kappa)}(\boldsymbol{E}^h, \boldsymbol{\phi}) = \int_{\tau_2(\kappa)} (E_3^h \frac{\partial \phi_2}{\partial x} - E_1^h \frac{\partial \phi_2}{\partial z})\, d\boldsymbol{x} - \int_{\partial\tau_2(\kappa)} (E_3^h n_1 - E_1^h n_3)\phi_2 \, ds.$$

Similarly, we multiply (2) by a test function $\boldsymbol{\phi} = (0, 0, \phi_3)^t$ with $\phi_3 \in U_3$, integrate the resulting equation on a macro cell $\tau_3(\kappa)$ and finally replace exact solutions by DG solutions to obtain

$$\int_{\tau_3(\kappa)} \mu \frac{\partial H_3^h}{\partial t}\, \phi_3 \, d\boldsymbol{x} + \Big\{ \int_{\tau_3(\kappa)} (E_1^h \frac{\partial \phi_3}{\partial y} - E_2^h \frac{\partial \phi_3}{\partial x})\, d\boldsymbol{x} - \int_{\partial\tau_3(\kappa)} (E_1^h n_2 - E_2^h n_1)\phi_3 \, ds \Big\} = 0. \tag{6}$$

We define

$$B_{\tau_3(\kappa)}(\boldsymbol{E}^h, \boldsymbol{\phi}) = \int_{\tau_3(\kappa)} (E_1^h \frac{\partial \phi_3}{\partial y} - E_2^h \frac{\partial \phi_3}{\partial x})\, d\boldsymbol{x} - \int_{\partial\tau_3(\kappa)} (E_1^h n_2 - E_2^h n_1)\phi_3 \, ds.$$

We write $\boldsymbol{J} = (J_1, J_2, J_3)^t$. Notice that $\tau_1(\sigma), \tau_2(\sigma)$ and $\tau_3(\sigma)$ are macro cells that are defined with respect to the edges of the initial grid that are parallel to the x-, y- and z-axis respectively. Taking a test function $\boldsymbol{\psi} = (\psi_1, 0, 0)^t$ with $\psi_1 \in W_1$, we multiply (1) by it and integrate the resulting equation over a macro cell $\tau_1(\sigma)$ to obtain

$$\int_{\tau_1(\sigma)} \varepsilon \frac{\partial E_1}{\partial t}\, \psi_1 \, d\boldsymbol{x} - \int_{\tau_1(\sigma)} (\frac{\partial H_3}{\partial y} - \frac{\partial H_2}{\partial z})\, \psi_1 \, d\boldsymbol{x} = - \int_{\tau_1(\sigma)} J_1 \psi_1 \, d\boldsymbol{x}.$$

Using first the Green's identity and replacing next exact solutions by DG solutions, we have now

$$\begin{aligned}\int_{\tau_1(\sigma)} \varepsilon \frac{\partial E_1^h}{\partial t}\, \psi_1 \, d\boldsymbol{x} - \Big\{ \int_{\tau_1(\sigma)} (H_2^h \frac{\partial \psi_1}{\partial z} - H_3^h \frac{\partial \psi_1}{\partial y}) \, d\boldsymbol{x} \\ - \int_{\partial\tau_1(\sigma)} (H_2^h n_3 - H_3^h n_2)\psi_1 \, ds \Big\} \\ = - \int_{\tau_1(\sigma)} J_1 \psi_1 \, d\boldsymbol{x}.\end{aligned} \tag{7}$$

We define

$$C_{\tau_1(\sigma)}(\boldsymbol{H}^h, \boldsymbol{\psi}) = \int_{\tau_1(\sigma)} (H_2^h \frac{\partial \psi_1}{\partial z} - H_3^h \frac{\partial \psi_1}{\partial y}) \, d\boldsymbol{x} - \int_{\partial\tau_1(\sigma)} (H_2^h n_3 - H_3^h n_2)\psi_1 \, ds.$$

In the same way, taking a test function $\boldsymbol{\psi} = (0, \psi_2, 0)^t$, with $\psi_2 \in W_2$, we get over a macro cell $\tau_2(\sigma)$

$$\begin{aligned}\int_{\tau_2(\sigma)} \varepsilon \frac{\partial E_2^h}{\partial t}\, \psi_2 \, d\boldsymbol{x} - \Big\{ \int_{\tau_2(\sigma)} (H_3^h \frac{\partial \psi_2}{\partial x} - H_1^h \frac{\partial \psi_2}{\partial z}) \, d\boldsymbol{x} \\ - \int_{\partial\tau_2(\sigma)} (H_3^h n_1 - H_1^h n_3)\psi_2 \, ds \Big\} \\ = - \int_{\tau_2(\sigma)} J_2 \psi_2 \, d\boldsymbol{x}.\end{aligned} \tag{8}$$

We define

$$C_{\tau_2(\sigma)}(\boldsymbol{H}^h, \boldsymbol{\psi}) = \int_{\tau_2(\sigma)} (H_3^h \frac{\partial \psi_2}{\partial x} - H_1^h \frac{\partial \psi_2}{\partial z}) \, d\boldsymbol{x} - \int_{\partial\tau_2(\sigma)} (H_3^h n_1 - H_1^h n_3)\psi_2 \, ds$$

Similarly, taking a test function $\boldsymbol{\psi} = (0, 0, \psi_3)^t$, with $\psi_3 \in W_3$, we get over a macro cell $\tau_3(\sigma)$

$$\begin{aligned}\int_{\tau_3(\sigma)} \varepsilon \frac{\partial E_3^h}{\partial t}\, \psi_3 \, d\boldsymbol{x} - \Big\{ \int_{\tau_3(\sigma)} (H_1^h \frac{\partial \psi_3}{\partial y} - H_2^h \frac{\partial \psi_3}{\partial x}) \, d\boldsymbol{x} \\ - \int_{\partial\tau_3(\sigma)} (H_1^h n_2 - H_2^h n_1)\psi_3 \, ds \Big\} \\ = - \int_{\tau_3(\sigma)} J_3 \psi_3 \, d\boldsymbol{x}.\end{aligned} \tag{9}$$

We define

$$C_{\tau_3(\sigma)}(\boldsymbol{H}^h, \boldsymbol{\psi}) = \int_{\tau_3(\sigma)} (H_1^h \frac{\partial \psi_3}{\partial y} - H_2^h \frac{\partial \psi_3}{\partial x}) \, d\boldsymbol{x} - \int_{\partial\tau_3(\sigma)} (H_1^h n_2 - H_2^h n_1)\psi_3 \, ds.$$

The above equations (4)-(9) define our new staggered DG method. One key feature of our new method is that the solutions $\boldsymbol{H}^h$ and $\boldsymbol{E}^h$ appeared in the boundary integrals in (4)-(9) are well-defined, and hence no numerical flux is needed. As an illustration, we consider the boundary integrals in (7), the values of the corresponding components of $\boldsymbol{H}^h$ are continuous. For instance,

the first term of the boundary integral is

$$\begin{aligned}
&\int_{\partial\tau_1(\sigma)} H_2^h\, n_3\, \psi_1\, ds \\
=&\int_{x_i}^{x_{i+1}} \int_{y_{j-\frac{1}{2}}}^{y_{j+\frac{1}{2}}} H_2^h(x,y,z_{k+\frac{1}{2}})\psi_1(x,y,z_{k+\frac{1}{2}})\, dydx \\
&-\int_{x_i}^{x_{i+1}} \int_{y_{j-\frac{1}{2}}}^{y_{j+\frac{1}{2}}} H_2^h(x,y,z_{k-\frac{1}{2}})\psi_1(x,y,z_{k-\frac{1}{2}})\, dydx
\end{aligned}$$

which requires continuity of H_2^h with respect to the z-variable so that it can be well-defined. By the definition of $\tau_2(\kappa)$, we see that the above integral corresponds to the integration on some of the internal faces of $\tau_2(\kappa)$, and on these faces, H_2^h is continuous with respect to the x and z variables.

The perfectly conducting boundary condition $\boldsymbol{E}\times\boldsymbol{n}=0$ on $\partial\Omega$, where $\boldsymbol{n}$ is the unit outward normal vector to $\partial\Omega$, is imposed *strongly* in the finite element spaces W_1, W_2 and W_3. We will illustrate this for W_1. Let σ be an edge that is parallel to the x-axis and let $\tau_1(\sigma)$ be the corresponding macro cell. Since σ lies on the domain boundary $\partial\Omega$, part of $\tau_1(\sigma)$ is outside Ω. Thus, the degrees of freedom that are located outside of Ω are set to zero. To impose the boundary condition for E_1, we set the degrees of freedom that lie on the intersection of $\tau_1(\sigma)$ and the domain boundary $\partial\Omega$ to zero. Therefore, E_1 is identically equal to zero on all inner faces of $\tau_1(\sigma)$ that also belong to the domain boundary $\partial\Omega$. We use the same method respectively for W_2 and W_3. As a result, we have enforced strongly the boundary condition $\boldsymbol{E}\times\boldsymbol{n}=0$ on $\partial\Omega$.

We will use the classical leap-frog scheme for the time discretization of (4)-(6) and (7)-(9). For a given time step $\Delta t>0$ and integers $n=0,1,2,\cdots$, the magnetic field $\boldsymbol{H}^h$ will be approximated at times $n\Delta t$ and are denoted by $\boldsymbol{H}^{h,n}$. Similarly, the electric field $\boldsymbol{E}^h$ will be approximated at times $(n+\frac{1}{2})\Delta t$ and are denoted by $\boldsymbol{E}^{h,n+\frac{1}{2}}$. Equation (4) is discretized as follows:

$$\begin{aligned}
&\int_{\tau_1(\kappa)} \mu\frac{H_1^{h,n+1}-H_1^{h,n}}{\Delta t}\,\phi_1\, d\boldsymbol{x} \\
+&\Big\{\int_{\tau_1(\kappa)} (E_2^{h,n+\frac{1}{2}}\frac{\partial\phi_1}{\partial z}-E_3^{h,n+\frac{1}{2}}\frac{\partial\phi_1}{\partial y})\, d\boldsymbol{x}-\int_{\partial\tau_1(\kappa)}(E_2^{h,n+\frac{1}{2}}n_3-E_3^{h,n+\frac{1}{2}}n_2)\phi_1\, ds\Big\}=0\,.
\end{aligned}\tag{10}$$

Equations (5) and (6) are discretized in a similar way. For (7), we use the following discretization

$$\begin{aligned}
&\int_{\tau_1(\sigma)} \varepsilon\frac{E_1^{h,n+\frac{3}{2}}-E_1^{h,n+\frac{1}{2}}}{\Delta t}\,\psi_1\, d\boldsymbol{x} \\
&-\Big\{\int_{\tau_1(\sigma)} (H_2^{h,n+1}\frac{\partial\psi_1}{\partial z}-H_3^{h,n+1}\frac{\partial\psi_1}{\partial y})\, d\boldsymbol{x}-\int_{\partial\tau_1(\sigma)}(H_2^{h,n+1}n_3-H_3^{h,n+1}n_2)\psi_1\, ds\Big\} \\
=&-\int_{\tau_1(\sigma)} J_1((n+1)\Delta t)\psi_1\, d\boldsymbol{x}.
\end{aligned}\tag{11}$$

This discretization is also used in (8) and (9). Therefore, given $(\boldsymbol{H}^{h,n},\boldsymbol{E}^{h,n+\frac{1}{2}})$, we can find the numerical solution at the next time level $(\boldsymbol{H}^{h,n+1},\boldsymbol{E}^{h,n+\frac{3}{2}})$ by solving (10), (11) and similar equations obtained from (5)-(6) and (8)-(9). It is well-known that this is a second order in time approximation. Notice that since our basis functions in the spaces U_i and W_i, $i=1,2,3$, are orthogonal, the resulting mass matrices are automatically diagonal. Hence, the above time discretization will result in an explicit scheme.

4. Energy conservation and discrete Gauss law

As we mentioned in the Introduction, our new staggered DG method is able to preserve the electromagnetic energy as well as a discrete version of the Gauss law, which are desirable for the numerical solutions of Maxwell's equations in the time domain and are the main advantages of our new method. In the following, we will prove these two results.

4.1. Energy conservation

In this section, we will show that our DG scheme (4)-(9) preserves the electromagnetic energy defined by

$$\mathcal{E}(\boldsymbol{H},\boldsymbol{E}) = \int_\Omega \left(\mu|\boldsymbol{H}|^2 + \varepsilon|\boldsymbol{E}|^2\right) d\boldsymbol{x}.$$

To prove the energy conservation, we will take $\phi_i = H_i^h$, $i = 1,2,3$, in equations (4), (5) and (6) respectively, and take $\psi_i = E_i^h$, $i = 1,2,3$, in equations (7), (8) and (9) respectively, and then add all equations together to obtain

$$\int_\Omega \left\{ \mu \frac{\partial \boldsymbol{H}^h}{\partial t} \cdot \boldsymbol{H}^h + \varepsilon \frac{\partial \boldsymbol{E}^h}{\partial t} \cdot \boldsymbol{E}^h \right\} d\boldsymbol{x} = -\int_\Omega \boldsymbol{J} \cdot \boldsymbol{E}^h \, d\boldsymbol{x}. \tag{12}$$

When $\boldsymbol{J} = \boldsymbol{0}$, we obtain

$$\frac{d}{dt}\mathcal{E}(\boldsymbol{H}^h,\boldsymbol{E}^h) = 0$$

which says that the electromagnetic energy is conserved. We observe that in order to obtain (12), all terms in (4)-(9) related to the curl operator (that is, all terms between brackets involving spatial derivatives and surface integrals) have to be cancelled. This is illustrated in the following paragraphs.

Taking $\phi_1 = H_1^h$ in equation (4) yields

$$\int_{\tau_1(\kappa)} \mu \frac{\partial H_1^h}{\partial t} H_1^h \, d\boldsymbol{x} + \Big\{ \int_{\tau_1(\kappa)} (E_2^h \frac{\partial H_1^h}{\partial z} - E_3^h \frac{\partial H_1^h}{\partial y}) \, d\boldsymbol{x} - \int_{\partial\tau_1(\kappa)} (E_2^h n_3 - E_3^h n_2) H_1^h \, ds \Big\} = 0. \tag{13}$$

We recall that $\tau_1(\kappa)$ is a union of 8 sub-cells. Consider one of the 8 sub-cells $\tau := [x_{i-\frac{1}{2}}, x_i] \times [y_j, y_{j+\frac{1}{2}}] \times [z_k, z_{k+\frac{1}{2}}]$ and only the terms between brackets. From (13), all these terms that are defined on τ or its boundary are

$$I := \int_\tau (E_2^h \frac{\partial H_1^h}{\partial z} - E_3^h \frac{\partial H_1^h}{\partial y}) \, d\boldsymbol{x} - \int_{\kappa_1\cup\kappa_2\cup\kappa_3} (E_2^h n_3 - E_3^h n_2) H_1^h \, ds$$

where κ_1, κ_2 and κ_3 are the three faces of τ defined by

$$\begin{aligned}
\kappa_1 &= \{x = x_{i-\frac{1}{2}}\} \times [y_j, y_{j+\frac{1}{2}}] \times [z_k, z_{k+\frac{1}{2}}], \\
\kappa_2 &= [x_{i-\frac{1}{2}}, x_i] \times \{y = y_j\} \times [z_k, z_{k+\frac{1}{2}}], \\
\kappa_3 &= [x_{i-\frac{1}{2}}, x_i] \times [y_j, y_{j+\frac{1}{2}}] \times \{z = z_k\}.
\end{aligned}$$

Remark that the approximate solutions E_2^h, E_3^h and H_1^h are all smooth over τ. Then, using the Green's formula for I, we get

$$I = \int_\tau H_1^h (\frac{\partial E_3^h}{\partial y} - \frac{\partial E_2^h}{\partial z}) \, d\boldsymbol{x} + \int_{\kappa_4\cup\kappa_5\cup\kappa_6} (E_2^h n_3 - E_3^h n_2) H_1^h \, ds := I_1 + I_2 \tag{14}$$

where κ_4, κ_5 and κ_6 are the remaining faces of τ:

$$\kappa_4 = \{x = x_i\} \times [y_j, y_{j+\frac{1}{2}}] \times [z_k, z_{k+\frac{1}{2}}],$$
$$\kappa_5 = [x_{i-\frac{1}{2}}, x_i] \times \{y = y_{j+\frac{1}{2}}\} \times [z_k, z_{k+\frac{1}{2}}],$$
$$\kappa_6 = [x_{i-\frac{1}{2}}, x_i] \times [y_j, y_{j+\frac{1}{2}}] \times \{z = z_{k+\frac{1}{2}}\}.$$

For I_2, we have both $n_2 = n_3 = 0$ on κ_4 and therefore there is no contribution on κ_4. On κ_5, we have $n_2 = 1$, $n_3 = 0$, while on κ_6, we have $n_2 = 0$, $n_3 = 1$. Thus,

$$I_2 = \int_{\kappa_5} (-E_3^h) H_1^h \, ds + \int_{\kappa_6} (E_2^h) H_1^h \, ds.$$

Similar results hold for the other seven sub-cells. Summarizing, (13) becomes

$$\int_{\tau_1(\kappa)} \mu \frac{\partial H_1^h}{\partial t} H_1^h \, d\boldsymbol{x} + \Big\{ \int_{\tau_1(\kappa)} H_1^h (\frac{\partial E_3^h}{\partial y} - \frac{\partial E_2^h}{\partial z}) \, d\boldsymbol{x} + \int_{\{y = y_{j+\frac{1}{2}}\} \cap \tau_1(\kappa)} [E_3^h] H_1^h \, ds - \int_{\{z = z_{k+\frac{1}{2}}\} \cap \tau_1(\kappa)} [E_2^h] H_1^h \, ds \Big\} = 0$$

where $\{y = y_{j+\frac{1}{2}}\}$ denotes the union of all faces with y-coordinate equals $y_{j+\frac{1}{2}}$ and $\{z = z_{k+\frac{1}{2}}\}$ denotes the union of all faces with z-coordinate equals $z_{k+\frac{1}{2}}$. Summing over all $\tau_1(\kappa)$, we obtain

$$\int_{\Omega} \mu \frac{\partial H_1^h}{\partial t} H_1^h \, d\boldsymbol{x} + \Big\{ \int_{\Omega} H_1^h (\frac{\partial E_3^h}{\partial y} - \frac{\partial E_2^h}{\partial z}) \, d\boldsymbol{x} + \sum_j \int_{\{y = y_{j+\frac{1}{2}}\}} [E_3^h] H_1^h \, ds - \sum_k \int_{\{z = z_{k+\frac{1}{2}}\}} [E_2^h] H_1^h \, ds \Big\} = 0. \tag{15}$$

By the same arguments, one can show that (5) with $\phi_2 = H_2^h$ can be written as

$$\int_{\Omega} \mu \frac{\partial H_2^h}{\partial t} H_2^h \, d\boldsymbol{x} + \Big\{ \int_{\Omega} H_2^h (\frac{\partial E_1^h}{\partial z} - \frac{\partial E_3^h}{\partial x}) \, d\boldsymbol{x} + \sum_k \int_{\{z = z_{k+\frac{1}{2}}\}} [E_1^h] H_2^h \, ds - \sum_i \int_{\{x = x_{i+\frac{1}{2}}\}} [E_1^h] H_2^h \, ds \Big\} = 0 \tag{16}$$

and (6) with $\phi_3 = H_3^h$ can be written as

$$\int_{\Omega} \mu \frac{\partial H_3^h}{\partial t} H_3^h \, d\boldsymbol{x} + \Big\{ \int_{\Omega} H_3^h (\frac{\partial E_2^h}{\partial x} - \frac{\partial E_1^h}{\partial y}) \, d\boldsymbol{x} + \sum_i \int_{\{x = x_{i+\frac{1}{2}}\}} [E_2^h] H_3^h \, ds - \sum_j \int_{\{y = y_{j+\frac{1}{2}}\}} [E_1^h] H_3^h \, ds \Big\} = 0 \tag{17}$$

where $\{x = x_{i+\frac{1}{2}}\}$ denotes the union of all faces with x-coordinate equals $x_{i+\frac{1}{2}}$. Next, we take $\psi_1 = E_1^h$ in (7) to get

$$\begin{aligned} &\int_{\tau_1(\sigma)} \varepsilon \frac{\partial E_1^h}{\partial t} E_1^h \, d\boldsymbol{x} - \Big\{ \int_{\tau_1(\sigma)} (H_2^h \frac{\partial E_1^h}{\partial z} - H_3^h \frac{\partial E_1^h}{\partial y}) \, d\boldsymbol{x} \\ &\quad - \int_{\partial \tau_1(\sigma)} (H_2^h n_3 - H_3^h n_2) E_1^h \, ds \Big\} \\ &= - \int_{\tau_1(\sigma)} J_1 E_1^h \, d\boldsymbol{x}. \end{aligned} \tag{18}$$

Summing over all $\tau_1(\sigma)$, we have

$$\begin{aligned}
&\int_\Omega \varepsilon \frac{\partial E_1^h}{\partial t} E_1^h \, d\boldsymbol{x} - \Big\{ \int_\Omega (H_2^h \frac{\partial E_1^h}{\partial z} - H_3^h \frac{\partial E_1^h}{\partial y}) \, d\boldsymbol{x} \\
&\quad + \sum_k \int_{\{z=z_{k+\frac{1}{2}}\}} H_2^h[E_1^h] \, ds - \sum_j \int_{\{y=y_{j+\frac{1}{2}}\}} H_3^h[E_1^h] \, ds \Big\} \\
&= - \int_\Omega J_1 E_1^h \, d\boldsymbol{x}.
\end{aligned} \tag{19}$$

Similarly, taking $\psi_2 = E_2^h$ in (8) and summing over all $\tau_2(\sigma)$, we get

$$\begin{aligned}
&\int_\Omega \varepsilon \frac{\partial E_2^h}{\partial t} E_2^h \, d\boldsymbol{x} - \Big\{ \int_\Omega (H_3^h \frac{\partial E_2^h}{\partial x} - H_1^h \frac{\partial E_2^h}{\partial z}) \, d\boldsymbol{x} \\
&\quad + \sum_i \int_{\{x=x_{i+\frac{1}{2}}\}} H_3^h[E_2^h] \, ds - \sum_k \int_{\{z=z_{k+\frac{1}{2}}\}} H_1^h[E_2^h] \, ds \Big\} \\
&= - \int_\Omega J_2 E_2^h \, d\boldsymbol{x}
\end{aligned} \tag{20}$$

while taking $\psi_3 = E_3^h$ in (9) and summing over all $\tau_3(\sigma)$, we get

$$\begin{aligned}
&\int_\Omega \varepsilon \frac{\partial E_3^h}{\partial t} E_3^h \, d\boldsymbol{x} - \Big\{ \int_\Omega (H_1^h \frac{\partial E_3^h}{\partial y} - H_2^h \frac{\partial E_3^h}{\partial x}) \, d\boldsymbol{x} \\
&\quad + \sum_j \int_{\{y=y_{j+\frac{1}{2}}\}} H_1^h[E_3^h] \, ds - \sum_i \int_{\{x=x_{i+\frac{1}{2}}\}} H_2^h[E_3^h] \, ds \Big\} \\
&= - \int_\Omega J_3 E_3^h \, d\boldsymbol{x}.
\end{aligned} \tag{21}$$

Finally, adding (15)-(17) and (19)-(21), we obtain (12).

From the above calculation, we see that

$$\begin{aligned}
&\sum_\kappa \Big\{ B_{\tau_1(\kappa)}(\tilde{\boldsymbol{E}}, \boldsymbol{\phi}) + B_{\tau_2(\kappa)}(\tilde{\boldsymbol{E}}, \boldsymbol{\phi}) + B_{\tau_3(\kappa)}(\tilde{\boldsymbol{E}}, \boldsymbol{\phi}) \Big\} \\
&+ \sum_\sigma \Big\{ C_{\tau_1(\sigma)}(\tilde{\boldsymbol{H}}, \boldsymbol{\psi}) + C_{\tau_2(\sigma)}(\tilde{\boldsymbol{H}}, \boldsymbol{\psi}) + C_{\tau_3(\sigma)}(\tilde{\boldsymbol{H}}, \boldsymbol{\psi}) \Big\} = 0
\end{aligned} \tag{22}$$

for all $\tilde{\boldsymbol{H}}, \boldsymbol{\phi} \in U_1 \times U_2 \times U_3$ and $\tilde{\boldsymbol{E}}, \boldsymbol{\psi} \in W_1 \times W_2 \times W_3$.

4.2. Discrete Gauss law

In this section, we will prove a discrete version of Gauss law for the first type element with polynomial order $p \geq 0$. We recall that our initial grid is defined by using the nodal points x_i, y_j, z_k where $i, j, k = 0, 1, 2, \cdots$. Using this initial grid, we define the *refined grid* by using the nodal points $x_i, x_{i+\frac{1}{2}}, y_j, y_{j+\frac{1}{2}}, z_k, z_{k+\frac{1}{2}}$ where $i, j, k = 0, 1, 2, \cdots$. Thus, the refined grid is obtained by uniformly subdividing each cell in the initial grid into eight cells. Let Q_{p+1}^c be the space of globally continuous piecewise polynomials with degree $p+1$ in each variable with respect to the refined grid. That is, Q_{p+1}^c is the quadrilateral conforming finite element space with respect to the refined grid. Let $q \in Q_{p+1}^c$ with the condition that $q = 0$ on $\partial\Omega$. Then it is easy to see that the first component of ∇q

is continuous in the y, z variables, the second component of ∇q is continuous in the x, z variables and the third component of ∇q is continuous in the x, y variables. Moreover, in each cell of the refined grid, we have $\nabla q \in Q_{p,p+1,p+1} \times Q_{p+1,p,p+1} \times Q_{p+1,p+1,p}$. Thus, ∇q belongs to the first type staggered DG space $W_1 \times W_2 \times W_3$. Taking the first component of ∇q as test function in (7) and by following the same steps in the derivation of (19), we have

$$\begin{aligned}
&\int_\Omega \varepsilon \frac{\partial E_1^h}{\partial t} (\nabla q)_1 \, d\boldsymbol{x} - \Big\{ \int_\Omega (H_2^h \frac{\partial (\nabla q)_1}{\partial z} - H_3^h \frac{\partial (\nabla q)_1}{\partial y}) \, d\boldsymbol{x} \\
&\quad + \sum_k \int_{\{z=z_{k+\frac{1}{2}}\}} H_2^h [(\nabla q)_1] \, ds - \sum_j \int_{\{y=y_{j+\frac{1}{2}}\}} H_3^h [(\nabla q)_1] \, ds \Big\} \\
&= - \int_\Omega J_1 (\nabla q)_1 \, d\boldsymbol{x}.
\end{aligned} \tag{23}$$

Similarly, taking the second component of ∇q as test function in (8) and by following the same steps in the derivation of (20), we have

$$\begin{aligned}
&\int_\Omega \varepsilon \frac{\partial E_2^h}{\partial t} (\nabla q)_2 \, d\boldsymbol{x} - \Big\{ \int_\Omega (H_3^h \frac{\partial (\nabla q)_2}{\partial x} - H_1^h \frac{\partial (\nabla q)_2}{\partial z}) \, d\boldsymbol{x} \\
&\quad + \sum_i \int_{\{x=x_{i+\frac{1}{2}}\}} H_3^h [(\nabla q)_2] \, ds - \sum_k \int_{\{z=z_{k+\frac{1}{2}}\}} H_1^h [(\nabla q)_2] \, ds \Big\} \\
&= - \int_\Omega J_2 (\nabla q)_2 \, d\boldsymbol{x}
\end{aligned} \tag{24}$$

In the same way, for the third component, we have

$$\begin{aligned}
&\int_\Omega \varepsilon \frac{\partial E_3^h}{\partial t} (\nabla q)_3 \, d\boldsymbol{x} - \Big\{ \int_\Omega (H_1^h \frac{\partial (\nabla q)_3}{\partial y} - H_2^h \frac{\partial (\nabla q)_3}{\partial x}) \, d\boldsymbol{x} \\
&\quad + \sum_j \int_{\{y=y_{j+\frac{1}{2}}\}} H_1^h [(\nabla q)_3] \, ds - \sum_i \int_{\{x=x_{i+\frac{1}{2}}\}} H_2^h [(\nabla q)_3] \, ds \Big\} \\
&= - \int_\Omega J_3 (\nabla q)_3 \, d\boldsymbol{x}.
\end{aligned} \tag{25}$$

Adding (23)-(25) and using the continuity properties of ∇q, we obtain the following discrete version of the Gauss law for the electric field

$$\int_\Omega \varepsilon \frac{\partial \boldsymbol{E}^h}{\partial t} \cdot \nabla q \, d\boldsymbol{x} = - \int_\Omega \boldsymbol{J} \cdot \nabla q \, d\boldsymbol{x}.$$

Similarly, by taking $q \in Q_{p+1}^c$, we get

$$\int_\Omega \mu \frac{\partial \boldsymbol{H}^h}{\partial t} \cdot \nabla q \, d\boldsymbol{x} = 0$$

which is a discrete version of the Gauss law for the magnetic field.

5. Error analysis

In this section, we will prove the optimal convergence and superconvergence of our new staggered DG method, defined by (4)-(9).

From (3) and (4), we obtain the error relation

$$\int_{\tau_1(\kappa)} \mu \frac{\partial(H_1 - H_1^h)}{\partial t}\, \phi_1 \, d\boldsymbol{x} + B_{\tau_1(\kappa)}(\boldsymbol{E} - \boldsymbol{E}^h, \boldsymbol{\phi}) = 0\,. \tag{26}$$

Let $\tilde{\boldsymbol{E}}$ be the interpolant of $\boldsymbol{E}$, that is, $\tilde{\boldsymbol{E}}$ belongs to our staggered DG spaces and has the same value as $\boldsymbol{E}$ at the interpolation points. Then

$$\int_{\tau_1(\kappa)} \mu \frac{\partial(H_1 - H_1^h)}{\partial t}\, \phi_1 \, d\boldsymbol{x} + B_{\tau_1(\kappa)}(\tilde{\boldsymbol{E}} - \boldsymbol{E}^h, \boldsymbol{\phi}) = -B_{\tau_1(\kappa)}(\boldsymbol{E} - \tilde{\boldsymbol{E}}, \boldsymbol{\phi})\,.$$

Similar relations hold for (5)-(6) and (7)-(9). Adding these results and using (22), we have

$$\begin{aligned}
&\frac{1}{2}\frac{d}{dt}\int_\Omega \left(\mu|\tilde{\boldsymbol{H}} - \boldsymbol{H}^h|^2 + \varepsilon|\tilde{\boldsymbol{E}} - \boldsymbol{E}^h|^2\right) d\boldsymbol{x} \\
=& -\int_\Omega \mu \frac{\partial(\boldsymbol{H} - \tilde{\boldsymbol{H}})}{\partial t}\,(\tilde{\boldsymbol{H}} - \boldsymbol{H}^h)\, d\boldsymbol{x} - \int_\Omega \varepsilon \frac{\partial(\boldsymbol{E} - \tilde{\boldsymbol{E}})}{\partial t}\,(\tilde{\boldsymbol{E}} - \boldsymbol{E}^h)\, d\boldsymbol{x} \\
&- \sum_\kappa \sum_{i=1}^{3} B_{\tau_i(\kappa)}(\boldsymbol{E} - \tilde{\boldsymbol{E}}, \tilde{\boldsymbol{H}} - \boldsymbol{H}^h) - \sum_\sigma \sum_{i=1}^{3} C_{\tau_i(\sigma)}(\boldsymbol{H} - \tilde{\boldsymbol{H}}, \tilde{\boldsymbol{E}} - \boldsymbol{E}^h)
\end{aligned} \tag{27}$$

where the last two summations are taken over all faces and edges in the initial grid respectively. Let τ be a generic cell in the refined grid. We first observe that, for the second type elements with polynomial order $p \geq 0$, by definition,

$$\int_\tau \mu \frac{\partial(\boldsymbol{H} - \tilde{\boldsymbol{H}})}{\partial t}\,(\tilde{\boldsymbol{H}} - \boldsymbol{H}^h)\, d\boldsymbol{x}$$

vanishes for functions $\boldsymbol{H}$ in $(Q_p)^3$, since in this case $\boldsymbol{H} = \tilde{\boldsymbol{H}}$ everywhere in τ. For the first type element with polynomial order $p \geq 1$, the above functional also vanishes for any $\boldsymbol{H} \in (Q_p)^3$ by the Gaussian and Radau quadrature rules since $\boldsymbol{H} = \tilde{\boldsymbol{H}}$ at the interpolation nodes and the quadrature rules exactly integrate polynomials of degrees $2p-1$ and $2p$ respectively. Hence, by the Bramble-Hilbert lemma, we obtain

$$\int_\tau \mu \frac{\partial(\boldsymbol{H} - \tilde{\boldsymbol{H}})}{\partial t}\,(\tilde{\boldsymbol{H}} - \boldsymbol{H}^h)\, d\boldsymbol{x} \leq Ch^{p+1}|\boldsymbol{H}_t|_{H^{p+1}(\tau)^3}\|\tilde{\boldsymbol{H}} - \boldsymbol{H}^h\|_{L^2(\tau)^3}$$

where the subscript t represents time derivative. Summing over all cells, we obtain

$$\int_\Omega \mu \frac{\partial(\boldsymbol{H} - \tilde{\boldsymbol{H}})}{\partial t}\,(\tilde{\boldsymbol{H}} - \boldsymbol{H}^h)\, d\boldsymbol{x} \leq Ch^{p+1}|\boldsymbol{H}_t|_{H^{p+1}(\Omega)^3}\|\tilde{\boldsymbol{H}} - \boldsymbol{H}^h\|_{L^2(\Omega)^3}.$$

Similarly, we have

$$\int_\Omega \varepsilon \frac{\partial(\boldsymbol{E} - \tilde{\boldsymbol{E}})}{\partial t}\,(\tilde{\boldsymbol{E}} - \boldsymbol{E}^h)\, d\boldsymbol{x} \leq Ch^{p+1}|\boldsymbol{E}_t|_{H^{p+1}(\Omega)^3}\|\tilde{\boldsymbol{E}} - \boldsymbol{E}^h\|_{L^2(\Omega)^3}.$$

In the following, we will estimate the remaining two terms in (27).

To find an upper bound for the last two terms of (27), it suffices to consider the following

$$\begin{aligned}
R :=& \int_{\tau_1(\kappa)} \left((E_2 - \tilde{E}_2)\frac{\partial \phi_1}{\partial z} - (E_3 - \tilde{E}_3)\frac{\partial \phi_1}{\partial y}\right) d\boldsymbol{x} \\
&- \int_{\partial\tau_1(\kappa)} \Big((E_2 - \tilde{E}_2)n_3 - (E_3 - \tilde{E}_3)n_2\Big)\phi_1 \, ds.
\end{aligned}$$

Other terms can be estimated in a similar fashion. Notice that, in the definition of R, we use ϕ_1 to replace the first component of $\tilde{\boldsymbol{H}} - \boldsymbol{H}^h$. By definition,

$$\tau_1(\kappa) = [x_{i-\frac{1}{2}}, x_{i+\frac{1}{2}}] \times [y_j, y_{j+1}] \times [z_k, z_{k+1}]$$

which is subdivided into 8 pieces by the center point $(x_i, y_{j+\frac{1}{2}}, z_{k+\frac{1}{2}})$. Using integration by parts, we have

$$\begin{aligned} R := &\int_{\tau_1(\kappa)} \Big(\phi_1 \frac{\partial}{\partial z}(E_2 - \tilde{E}_2) - \phi_1 \frac{\partial}{\partial y}(E_3 - \tilde{E}_3)\Big)\, d\boldsymbol{x} \\ &- \int_{\kappa_1} [E_2 - \tilde{E}_2]\, \phi_1 \, ds + \int_{\kappa_2} [E_3 - \tilde{E}_3]\, \phi_1 \, ds \end{aligned} \tag{28}$$

where $\kappa_1 := [x_{i-\frac{1}{2}}, x_{i+\frac{1}{2}}] \times [y_j, y_{j+1}] \times \{z = z_{k+\frac{1}{2}}\}$ and $\kappa_2 := [x_{i-\frac{1}{2}}, x_{i+\frac{1}{2}}] \times \{y = y_{j+\frac{1}{2}}\} \times [z_k, z_{k+1}]$. Now, we consider one of the 8 pieces $\tau' := [x_i, x_{i+\frac{1}{2}}] \times [y_{j+\frac{1}{2}}, y_{j+1}] \times [z_{k+\frac{1}{2}}, z_{k+1}]$. Collecting the terms involving this piece, we get

$$\begin{aligned} R' := &\int_{\tau'} \Big((E_2 - \tilde{E}_2)\frac{\partial \phi_1}{\partial z} - (E_3 - \tilde{E}_3)\frac{\partial \phi_1}{\partial y}\Big)\, d\boldsymbol{x} \\ &- \int_{\kappa_1' \cup \kappa_2' \cup \kappa_3'} \Big((E_2 - \tilde{E}_2)n_3 - (E_3 - \tilde{E}_3)n_2\Big)\phi_1 \, ds \end{aligned}$$

where

$$\begin{aligned} \kappa_1' &:= \{x = x_{i+\frac{1}{2}}\} \times [y_{j+\frac{1}{2}}, y_{j+1}] \times [z_{k+\frac{1}{2}}, z_{k+1}], \\ \kappa_2' &:= [x_i, x_{i+\frac{1}{2}}] \times \{y = y_{j+1}\} \times [z_{k+\frac{1}{2}}, z_{k+1}], \\ \kappa_3' &:= [x_i, x_{i+\frac{1}{2}}] \times [y_{j+\frac{1}{2}}, y_{j+1}] \times \{z = z_{k+1}\}. \end{aligned}$$

We note that κ_1', κ_2' and κ_3' are normal to the x, y and z axis respectively. Consequently, $n_2 = n_3 = 0$ on κ_1', $n_1 = n_3 = 0$ on κ_2' and $n_1 = n_2 = 0$ on κ_3'. Then R' becomes

$$\begin{aligned} R' := &\int_{\tau'} \Big((E_2 - \tilde{E}_2)\frac{\partial \phi_1}{\partial z} - (E_3 - \tilde{E}_3)\frac{\partial \phi_1}{\partial y}\Big)\, d\boldsymbol{x} \\ &- \int_{\kappa_2'} (E_3 - \tilde{E}_3) n_2 \phi_1 \, ds - \int_{\kappa_3'} (E_2 - \tilde{E}_2) n_3 \phi_1 \, ds. \end{aligned}$$

In the following, we will estimate R' for both the first and the second type elements.

For the first type element:

We first consider the integral $\int_{\tau'}(E_2 - \tilde{E}_2)\frac{\partial \phi_1}{\partial z}$. We recall that $\frac{\partial \phi_1}{\partial z} \in Q_{p-1,p,p-1}$ and $\tilde{E}_2 \in Q_{p,p-1,p}$. Moreover, the x and z coordinates of $\tilde{E}_2$ are defined using Radau points and the y coordinate of $\tilde{E}_2$ are defined using Gaussian points. Then, by using Radau and Gaussian quadrature rules, the integral vanishes for all functions E_2 in $Q_{p+1,p-1,p+1}$, since, in this case, the integrand belongs to $Q_{2p,2p-1,2p}$. Similarly, we have $\int_{\tau'}(E_3 - \tilde{E}_3)\frac{\partial \phi_1}{\partial y}$ vanishes for all functions E_3 in $Q_{p+1,p+1,p-1}$. Now we consider the two surface integrals in R'. Using the Radau quadrature for the x variable and the Gaussian quadrature for the z variable, we see that the integral $\int_{\kappa_3'}(E_2 - \tilde{E}_2)n_3\phi_1 \, ds$ vanishes when $E_2 \in Q_{p+1,p-1,p+1}$. Similarly, the integral $\int_{\kappa_2'}(E_3 - \tilde{E}_3)n_2\phi_1 \, ds$ vanishes for all E_3 in $Q_{p+1,p+1,p-1}$. Notice that, similar result hold for the other 7 pieces in R. Moreover, from (28), we see that $R = 0$

when $E_2 = y^m$ and $E_3 = z^m$ with $m = p, p+1$. Consequently, R vanishes for all polynomials of degree less than or equal to $p+1$. Hence, by the Bramble-Hilbert lemma, we obtain

$$R \leq Ch^{p+1}|\boldsymbol{E}|_{H^{p+2}(\tau_1(\kappa))^3}\|\phi_1\|_{L^2(\tau_1(\kappa))}.$$

For the second type element:

The proof for this case is essentially the same as the first type element. The main difference is that, for $\tilde{E}_2$, one more Gaussian point is used for the y variable and for $\tilde{E}_3$, one more Gaussian point is used for the z variable. By the same techniques, we see that $R' = 0$ for all functions E_2 and E_3 in $Q_{p+1,p,p+1}$ and $Q_{p+1,p+1,p}$ respectively. This is also true for the other 7 pieces. Moreover, from (28), we see that $R = 0$ when $E_2 = y^{p+1}$ and $E_3 = z^{p+1}$. Consequently, R vanishes for all polynomials of degree less than or equal to $p+1$. Hence, by the Bramble-Hilbert lemma, we obtain

$$R \leq Ch^{p+1}|\boldsymbol{E}|_{H^{p+2}(\tau_1(\kappa))^3}\|\phi_1\|_{L^2(\tau_1(\kappa))}.$$

Combining the above results, we obtain the following theorem.

Theorem 1. *Let $(\boldsymbol{H}^h, \boldsymbol{E}^h)$ be the solution of the staggered DG method and let $(\tilde{\boldsymbol{H}}, \tilde{\boldsymbol{E}})$ be the interpolant of the exact solution into the staggered DG space. Then we have*

$$\|\mu^{\frac{1}{2}}(\tilde{\boldsymbol{H}} - \boldsymbol{H}^h)\| + \|\varepsilon^{\frac{1}{2}}(\tilde{\boldsymbol{E}} - \boldsymbol{E}^h)\| \leq Ch^{p+1}.$$

In the above theorem, the norms on the left hand side are discrete L^2 norms measured at the interpolation points. Thus, for the first type element, this is a superconvergence result since the convergence rate is one order higher than that of the interpolation error. In the following theorem, we state the error estimates with respect to L^2 norm. The proof is based on the use of classical interpolation error estimates.

Theorem 2. *Let $(\boldsymbol{H}^h, \boldsymbol{E}^h)$ be the solution of the staggered DG method and let $(\boldsymbol{H}, \boldsymbol{E})$ be the exact solution. Then we have*

$$\|\mu^{\frac{1}{2}}(\boldsymbol{H} - \boldsymbol{H}^h)\| + \|\varepsilon^{\frac{1}{2}}(\boldsymbol{E} - \boldsymbol{E}^h)\| \leq Ch^{p}$$

for the first type element with $p \geq 1$ and

$$\|\mu^{\frac{1}{2}}(\boldsymbol{H} - \boldsymbol{H}^h)\| + \|\varepsilon^{\frac{1}{2}}(\boldsymbol{E} - \boldsymbol{E}^h)\| \leq Ch^{p+1}$$

for the second type element with $p \geq 0$.

6. Numerical examples

In this section, we will present numerical examples to validate the high order of convergence of our new DG method. Furthermore, we will provide results on simulation of wave diffraction by perfectly conducting objects. We will also present an example with an unbounded domain with the use of PML. For all examples below, we take the domain Ω to be $[0,1]^d$, $(d = 2, 3)$, and a uniform grid with $h = h_1 = h_2 = h_3$.

6.1. Convergence tests

In this section, we present a convergence rate test for a $3D$ problem to validate our estimates in Theorem 1 and Theorem 2. The exact solution of the problem is chosen as

$$\begin{aligned}
E_1(x,y,z,t) &= \sin(\pi t)\sin(\pi y)\sin(\pi z)\\
E_2(x,y,z,t) &= \sin(\pi t)\sin(\pi y)\sin(\pi z)\\
E_3(x,y,z,t) &= \sin(\pi t)\sin(\pi x)\sin(\pi y)\\
H_1(x,y,z,t) &= \sin(\pi x)\cos(\pi t)(\cos(\pi y)-\cos(\pi z))\\
H_2(x,y,z,t) &= -\sin(\pi y)\cos(\pi t)(-\cos(\pi z)+\cos(\pi x))\\
H_3(x,y,z,t) &= \sin(\pi z)\cos(\pi t)(\cos(\pi x)-\cos(\pi y))\\
J_1(x,y,z,t) &= -\pi\cos(\pi t)\sin(\pi y)\sin(\pi z)\\
J_2(x,y,z,t) &= -\pi\cos(\pi t)\sin(\pi x)\sin(\pi z)\\
J_3(x,y,z,t) &= -\pi\cos(\pi t)\sin(\pi x)\sin(\pi y)
\end{aligned}$$

We will compute the errors in L^2 and discrete L^2 norms using both types of elements with polynomial order $p = 1, 2$ and 3 at the time $T = 1.1$. The log-log plots of these errors against various mesh sizes are shown in Figure 2 and Figure 3, in which the dash lines represent the method with $p = 1$, the dash-dot lines represent the method with $p = 2$ and the solid lines represent the method with $p = 3$. In Figure 2 , the errors measured in L^2 norm (left) and discrete L^2 norm (right) are presented. We see that the order of convergence measured in the discrete L^2 norm is one order higher than the order measured in the L^2 norm. From Figure 3, we see that the order of convergence measured in both the L^2 and the discrete L^2 norms are the same. These confirm our estimates in Theorem 1 and Theorem 2.

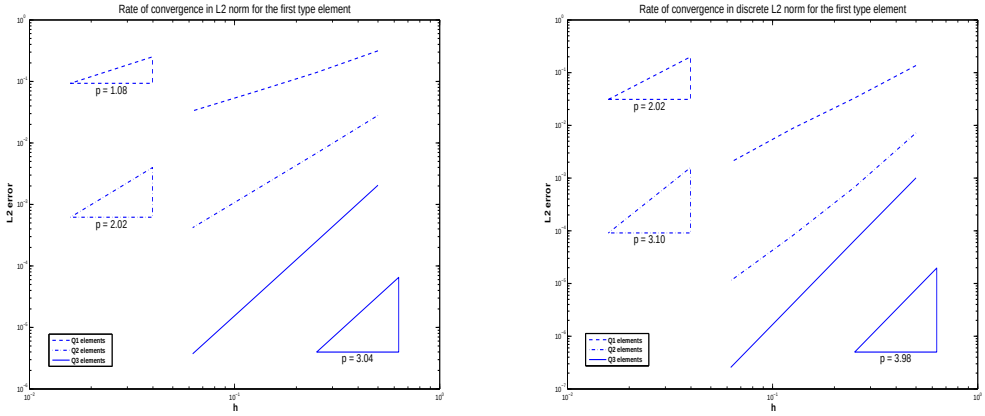

Figure 2: Rate of convergence in L^2 and discrete L^2 norms for the first type element.

6.2. Diffraction by a perfectly conducting object

In this section, we will present simulation results for wave diffraction problems by perfectly conducting objects. We will consider the TE mode in the domain $[0, 1]^2$ with perfectly conductor

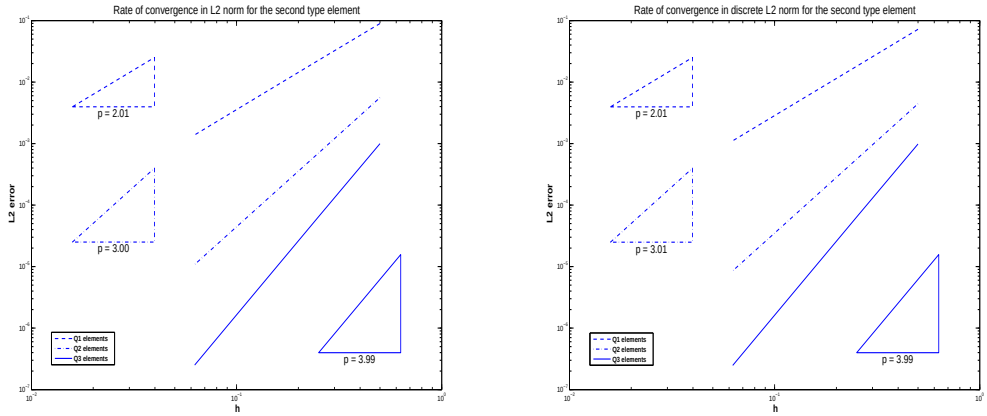

Figure 3: Rate of convergence in L^2 and discrete L^2 norms for the second type element.

boundary condition. The initial pulses are taken as $E_1(0) = E_2(0) = 0$ and

$$H_3(x, y, 0) = \begin{cases} \sin(16\pi x), & 0 \leq x \leq \frac{1}{8}, \\ 0, & \text{otherwise.} \end{cases}$$

The first example is the wave diffraction problem by a perfectly conducting object which is a square centered at $(0.5, 0.5)$ with width equal to 0.25, shown in Figure 4. In the following, we present the behavior of $H_3(x, y, t)$ as a function of t at three reference points defined respectively by $(0.125, 0.875)$, $(0.5, 0.875)$ and $(0.875, 0.875)$, shown again by black dots in Figure 4. The numerical simulations are computed by using our two types of DG methods with $p = 3$ and using a mesh size $h = 1/128$.

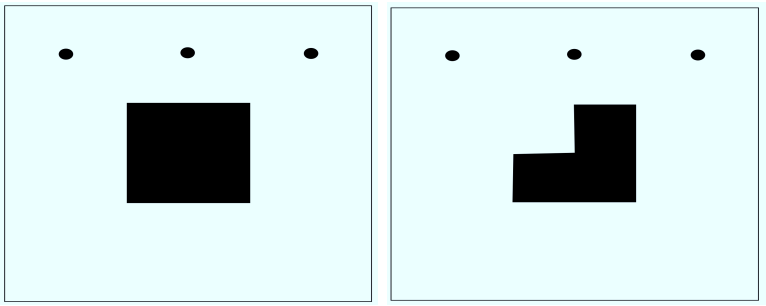

Figure 4: Wave diffraction problems. Left: square obstacle. Right: L-shaped obstacle.

In order to verify the accuracy of our method, we compare the numerical solution and the reference solution obtained by the FDTD method. The reference solution is computed by using a fine grid with mesh size $h = 1/2048$. In Figure 5, we present the numerical solutions obtained by our two types of DG methods and the reference solution at the three reference points. In these figures, we use solid line to represent the reference solution, dash-dot line to represent the numerical solution using the first type DG space and dash line to represent the numerical solution using the second type DG space It is clear that our method gives the correct behavior.

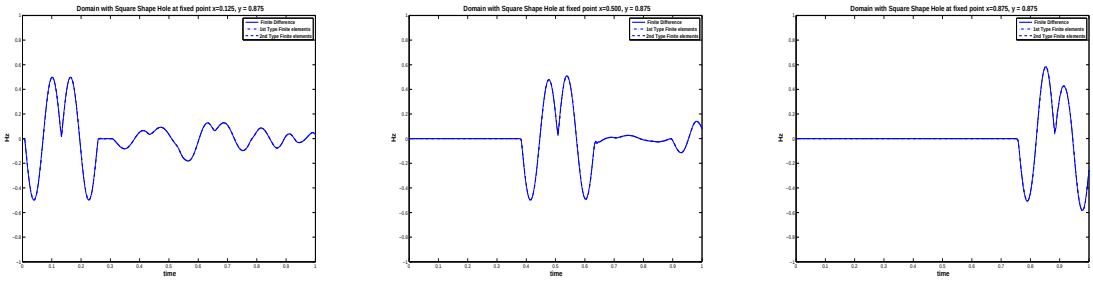

Figure 5: Square obstacle: comparision of our solution and the reference solution at the 3 reference points. Left: $(0.125, 0.875)$. Middle: $(0.5, 0.875)$. Right: $(0.875, 0.875)$.

Next, we perform a similar simulation by using a L-shaped perfectly conducting obstacle defined by $[0.25, 0.75]^2 \backslash ([0.25, 0.5] \times [0.5, 0.75])$ (see Figure 4). We again consider both the first and the second type elements with $p = 3$ and mesh size $h = 1/256$. The numerical and reference solutions are shown in Figure 6. We again see that our method gives the correct behavior.

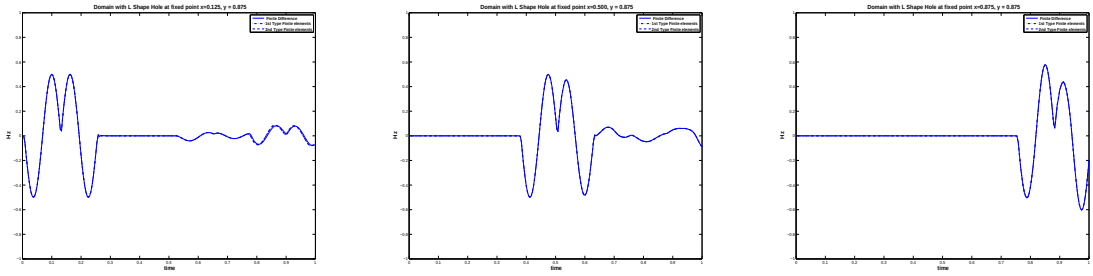

Figure 6: L-shaped obstacle: comparision of our solution and the reference solution at the 3 reference points. Left: $(0.125, 0.875)$. Middle: $(0.5, 0.875)$. Right: $(0.875, 0.875)$.

6.3. Perfectly matched layers

In this section, we will consider the wave propagation problem in an unbounded domain. The initial pulses are chosen as

$$E_1(x, y, 0) = E_2(x, y, 0) = 0 \quad \text{and} \quad H_3(x, y, 0) = e^{-100((x-0.5)^2+(y-0.5)^2)}.$$

We will apply PML (see Berenger [1]) in conjunction with our new DG method with $p = 1$. In order to test the accuracy of our method, we will compute a reference solution on a larger domain $[-0.5, 1.5]^2$ with only the perfectly conductor boundary condition. We then compute the difference between our solution and the reference solution in the original computational domain $[0, 1]^2$ at a time so that the wave does not hit the boundary of the enlarged domain $[-0.5, 1.5]^2$. In Figure 7, we present the errors computed by using the two types of DG methods. As we can see from these figures, the errors for both type of methods are very small (having magnitude of about 10^{-3}).

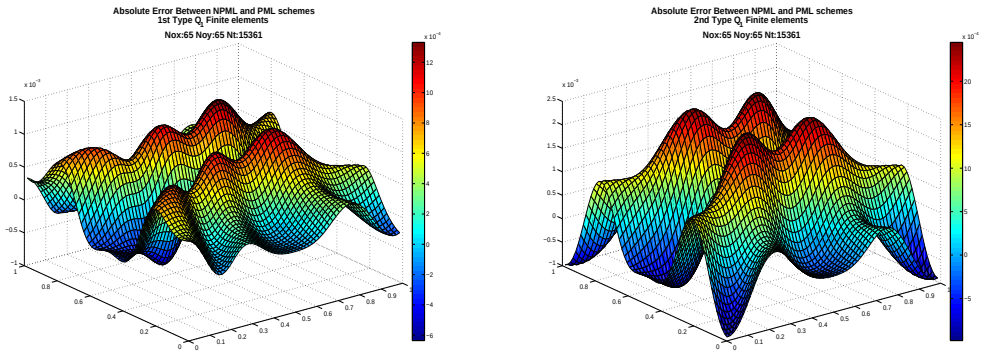

Figure 7: Errors for the unbounded domain example. Left: first type element. Right: second type element.

7. Conclusion

In this paper, we have developed and analyzed a new class of staggered DG method for the time-dependent Maxwell's equations. Two types of staggered DG spaces are proposed which generalize the classical Nedelec first and second family of finite elements. The new method has many advantages, namely, diagonal mass matrices, energy conservation as well as automatic fulfillment of Gauss law. Moreover, the method is high order accurate and the optimal error estimates are proved. A superconvergence result, stating the convergence rate at the interpolation nodes is one order higher, is also proved. Due to its Cartesian structure, the method is very easy to implement. Hence, our method gives an attractive alternative to existing technologies. In the future, we plan to develop and analyze these kind of staggered spaces for tetrahedral meshes.

Acknowledgements

Eric T. Chung would like to thank the Hong Kong Research Grant Council for supporting this research. (Project number: 401010).

References

[1] Berenger, J. P. *A perfectly matched layer for absorbing of electromagetic waves.* J. Comput. Phys., 114 (1994), pp. 185–200.

[2] Brenner, S. C., Li, F. & Sung, L.-Y. *A locally divergence-free interior penalty method for two-dimensional curl-curl problems.* SIAM J. Numer. Anal., 46 (2008), pp. 1190–1211.

[3] Brezzi, F., Marini, L. D., & Süli, E. *Discontinuous Galerkin methods for first-order hyperbolic problems.* Math. Models Methods Appl. Sci., 14 (2004), pp. 1893–1903.

[4] Buffa, A., Houston, P. & Perugia, I. *Discontinuous Galerkin computation of the Maxwell eigenvalues on simplicial meshes.* J. Comput. Appl. Math., 204 (2007), pp. 317–333.

[5] Buffa, A. & Perugia, I. *Discontinuous Galerkin approximation of the Maxwell eigenproblem.* SIAM J. Numer. Anal., 44 (2006), pp. 2198–2226.

[6] Chung, E. T. & Ciarlet, P. Jr. *Convergence of the staggered discontinuous Galerkin method for wave propagation between dielectrics and meta-materials*. Under review.

[7] Chung, E. T., Du, Q. & Zou, J. *Convergence analysis on a finite volume method for Maxwell's equations in non-homogeneous media*. SIAM J. Numer. Anal., 41 (2003), pp. 37–63.

[8] Chung, E. T. & Engquist, B. *Convergence analysis of fully discrete finite volume methods for Maxwell's equations in nonhomogeneous media*. SIAM J. Numer. Anal., 43 (2005), pp. 303–317.

[9] Chung, E. T. & Engquist, B. *Optimal discontinuous galerkin methods for wave propagation*. SIAM J. Numer. Anal., 44, pp. 2131–2158.

[10] Chung, E. T. & Engquist, B. *Optimal discontinuous galerkin methods for the acoustic wave equation in higher dimensions*. SIAM J. Numer. Anal., 47 (2009), pp. 3820–3848.

[11] Chung, E. T. & Lee, C. S. *A staggered discontinuous Galerkin method for the curl-curl operator*. IMA J. Numer. Anal., To appear.

[12] Chung, E. T. & Lee, C. S. (2011) *A staggered discontinuous Galerkin method for the convection-diffusion equation*. J. Numer. Math., To appear.

[13] Cockburn, B., Kanschat, G., Perugia, I. & Schötzau, D. *Superconvergence of the local discontinuous Galerkin method for elliptic problems on Cartesian grids*. SIAM J. Numer. Anal., 39 (2001), pp. 264–285.

[14] Cockburn, B. & Shu, C. W. *The local discontinuous Galerkin method for time-dependent convection-diffusion systems*. SIAM J. Numer. Anal., 35 (1998), pp. 2440–2463.

[15] Cohen, G. & Monk, P. *Gauss point mass lumping schemes for Maxwell's equations*. Numer. Methods Partial Differential Equations, 14 (1998), pp. 63–88.

[16] Costabel, M. & Dauge, M. *Singularities of electromagnetic fields in polyhedral domains*. Arch. Ration. Mech. Anal., 151 (2000), pp. 221–276.

[17] Dauge, M. *Computatons for Maxwell equations for the approximation of highly singular solution*.
http://perso.univ-rennes1.fr/monique.dauge/benchmax.html.

[18] Fezoui, L., Lanteri, S., Lohrengel, S. & Piperno, S. *Convergence and Stability of a Discontinuous Galerkin Time-Domain method for the 3D heterogeneous Maxwell equations on unstructured meshes*. M2AN, 39 (2005), pp. 1149–1176.

[19] Gittelson, C. J., Hiptmair, R. & Perugia, I. *Plane wave discontinuous Galerkin methods: analysis of the h-version*. M2AN Math. Model. Numer. Anal., 2 (2009), pp. 297–331.

[20] Grote, M., Schneebeli, A. & Schötzau, D. *Interior penalty discontinuous Galerkin methods for Maxwell's equations: Optimal L^2 norm error estimates*. IMA J. Numer. Anal., 28 (2008), pp. 440–468.

[21] Hesthaven, J. S. & Warburton, T. *High-order nodal methods on unstructured grids. I. Time-domain solution of Maxwells equations*. J. Comput. Phys., 181 (2002), pp.186–221.

[22] Hiptmair, R. *Finite elements in computational electromagnetics.* Acta Numerica, 11 (2002), pp. 237–339.

[23] Houston, P., Perugia, I., Schneebeli, A. & Schötzau, D. *Interior penalty method for the indefinite time-harmonic Maxwell equations.* Numer. Math., 100 (2005), pp. 485–518.

[24] Houston, P., Perugia, I., Schneebeli, A. & Schötzau, D. *Mixed discontinuous Galerkin approximation of the Maxwell operator: the indefinite case.* ESAIM: M2AN, 39 (2005), pp, 727–753.

[25] Houston, P., Perugia, I. & Schötzau, D. *Mixed discontinuous Galerkin approximation of the Maxwell operator.* SIAM J. Numer. Anal., 42 (2004), pp, 434–459.

[26] Huang, Y., Li, J., Yang, W. & Sun, S. *Superconvergence of mixed finite element approximations to 3-D Maxwells equations in metamaterials.* J. Comput. Phys., 230 (2011), pp. 8275–8289.

[27] Monk, P. *Finite element methods for Maxwells equations.* Oxford University Press, New York.

[28] Nedelec, J. *Mixed finite element in R^3.* Numer. Math., 35 (1980), pp. 315–341.

[29] Nedelec, J. *A new family of mixed finite elements in R^3.* Numer. Math., 50 (1986), pp. 57–81.

[30] Perugia, I., Schötzau, D. & Monk, P. *Stabilized interior penalty methods for the time-harmonic Maxwell equations.* Comput. Methods Appl. Mech. Eng., 191 (2002), pp. 4675–4697.

[31] Yee, K. S. *Numerical solution of initial boundary value problems involving Maxwells equations in isotropic media.* IEEE Trans. Antennas Propagat., 14 (1966), pp. 302–307.